

Probing the anisotropic expansion history of the universe with cosmic microwave background

Ranjita K. Mohapatra,^{*} P. S. Saumia,[†] and Ajit M. Srivastava[‡]
Institute of Physics, Sachivalaya Marg, Bhubaneswar 751005, India

We propose a simple technique to detect any anisotropic expansion stage in the history of the universe starting from the inflationary stage to the surface of last scattering from the CMBR data. We use the property that any anisotropic expansion in the universe would deform the shapes of the primordial density perturbations and this deformation can be detected in a shape analysis of superhorizon fluctuations in CMBR. Using this analysis we obtain the constraint on any previous anisotropic expansion of the universe to be less than about 35 %.

PACS numbers: 98.80.Cq, 98.80.Es

I. INTRODUCTION

Observations show that the present universe is homogeneous and isotropic on large scales. One of the most important observational evidences for the homogeneity and isotropy of the universe is the highly smooth and uniform cosmic microwave background radiation (CMBR). The distribution of matter in the universe is also generally consistent with a homogeneous and isotropic universe at present. However, this does not rule out the possibility of an anisotropic expansion of the universe during some early stage (say, during inflation) such that the expansion becomes isotropic later on. For example, the universe may have expanded anisotropically during the early stages of the inflation. If the expansion becomes isotropic subsequently (which is most likely to happen due to the no-hair theorem [1]), then it is not obvious whether any signatures of such an early, transient, stage of anisotropic expansion would be present in the present day universe. We ask the question whether one can put constraints on such an early, transient, stage of anisotropic expansion using CMBR data in, as much as possible, model independent way (e.g. not even assuming inflationary stage). We propose a technique for this which is based on analyzing the shapes of superhorizon sized fluctuations in CMBR at the surface of last scattering, i.e. patches of angular sizes larger than about 1 degree at the present stage. Due to being superhorizon until the last scattering stage, the shapes of these patches will undergo simple scaling in different directions, and hence will retain the memory of any anisotropic expansion stage in the entire history of the universe. Though even the subhorizon fluctuations in CMBR may retain this shape information due to linear evolution. However, for subhorizon fluctuations one cannot rule out various causal effects (such as the presence of magnetic fields) which may distort the shapes. Statistically such a distortion (from causal effects) may not be significant, however, it seems simpler to restrict to superhorizon fluctuations for the initial analysis.

Our technique is very general and does not depend on any specific models for describing the early universe stages. For example, even in the absence of any inflationary stage, the shapes of the density fluctuations patches at superhorizon scales will contain the memory of any anisotropic expansion stage. However, for the sake of definiteness, and with the general confidence in an inflationary paradigm, we will continue to refer to an early inflationary stage of the universe which is responsible for the generation of density fluctuations in the universe. Note also, though we talk about detecting anisotropic expansion, any other anisotropy which leaves its imprints in the universe in terms of shape deformations (for example if initial density fluctuations themselves were anisotropic) will also be detected by our technique. However, it is clearly important to know if one can distinguish between the anisotropy originating entirely from the initial conditions, and the one arising from anisotropic universe expansion. For example, in the inflationary paradigm, our entire observed universe has originated from a single causal patch. It seems entirely possible that initial fluctuations may be anisotropic due to the presence of some background field. Once these fluctuations go out of the horizon, they will then remain anisotropic, and will eventually manifest in the anisotropic shapes of patches of CMBR. (Though the effects of such a background field will diminish rapidly, hence fluctuations produced later on will be mostly isotropic.) One would like to distinguish such a situation of initial anisotropic fluctuations from the case when fluctuations are produced isotropically but undergo shape deformations due to anisotropic expansion of the

^{*}Electronic address: ranjita@iopb.res.in

[†]Electronic address: saumia@iopb.res.in

[‡]Electronic address: ajit@iopb.res.in

universe. (Even here, eventually the universe expansion becomes isotropic [1], hence any fluctuations produced after that will remain isotropic.)

We will discuss two different ways of identifying shape deformations of temperature fluctuation patches. We generate patches by considering some threshold value for overdensity (or underdensity) of CMBR fluctuations in a given region on the surface of last scattering. This will generate the excursion sets and we will get a picture of that region consisting of these excursion sets. We then study shape deformation of these excursion sets (patches) in this region using either the Fourier transform, or we detect it directly in the spatial patch. Both these methods can detect the shape deformations. However, direct shape analysis with spatial region has specific advantages which we will discuss later on. We have also analyzed simulated density fluctuations of specific geometrical shapes, such as spheres, ellipsoids. This helps us in analyzing the strengths of these two techniques in differentiating various scenarios, such as anisotropies arising from initial conditions, or anisotropies arising from the anisotropic expansion etc. We will show that this simple shape analysis is able to answer an important question in an almost model independent manner. That is whether the universe ever expanded anisotropically almost from the beginning of inflation near $t \simeq 10^{-35}$ sec. all the way up to the stage of last scattering when the universe was 300,000 years old.

The paper is organized in the following manner. In section II, we will briefly discuss some other techniques which have been used in the literature for studying the anisotropy of the universe. Section III discusses the method for generating the excursion sets for the shape analysis. Section IV discusses the shape anisotropy analysis using Fourier transforms. In section V we describe our method for analyzing shape anisotropy directly in the spatial region. Section VI discusses applications of these techniques to detect anisotropic expansion by artificially stretching the CMBR data in one direction. Using different stretching factors we constrain the anisotropic expansion factor of the universe. Section VII discusses the analysis with simulated fluctuations of definite geometric shapes and sizes. Different cases are analyzed to distinguish different scenarios leading to anisotropic shapes of fluctuations in the universe. Conclusions are presented in section VIII.

II. OTHER PROBES OF THE ANISOTROPY OF THE UNIVERSE

The density perturbations resulting from the general inflationary picture (consequently temperature fluctuations in CMBR) are expected to be statistically homogeneous and isotropic Gaussian random fluctuations around a uniform background. Many people have discussed departures from the isotropy. Non-Gaussianity is an important probe of various inflationary models as well as contributions from other sources of density fluctuations, and is being intensively investigated. Regarding the isotropy of the universe, recently there have been claims of evidences of statistical anisotropy in CMBR [2, 3] on large angular scales. These evidences are more of the nature of identifying a special direction (axis) in the CMBR sky [3] which shows excess power in specific m modes in the multipole expansion of temperature fluctuations. Various suggested explanations for this statistical anisotropy include nontrivial topology of the universe [4] and anisotropic expansion. As we mentioned, the anisotropy discussed in these works corresponds to large angular scales, e.g. referring to the alignment of quadrupole and octupole moments in the CMBR sky. In contrast, our analysis method probes anisotropy at relatively shorter angular scales from 1° to about 20° (as we will explain below).

There are other techniques, e.g. Minkowski functionals [5] which have been used for analyzing CMBR fluctuations (e.g. non-Gaussianity [6]) and morphological and topological properties of matter distribution in the universe [7]. These techniques are very useful in providing structural properties of density fluctuations. For example, *shapefinders* can yield statistics of filamentary or pancake structures. These techniques have also been used in diverse areas, e.g. for investigating geometry and topology of the excursion sets (with a given threshold) for the magnetic field of the Sun [8]. Such techniques applied to CMBR excursion sets will also lead to useful information about the nature of density fluctuations, for example Gaussianity, geometry and topology of excursion sets, etc. However, an overall shape deformation of fluctuations arising from anisotropic universe expansion is an entirely different issue and Minkowski functionals have not been used to analyze this issue. For example, a randomly oriented collection of filamentary structures (or pancake structures) will be detected using shapefinders, but it does not imply anisotropic expansion of the universe which will require an overall alignment of the orientation of such structures. Our purpose is to detect such an overall alignment of (statistically) non-spherical structures. Similar situation is with other techniques which have been used in the literature to study topological features of CMBR fluctuations. For example, the genus statistics of excursion sets of CMBR fluctuations has been used to detect non-Gaussianity [9]. However, here also any possibility of an overall orientation is not investigated. In this context we mention that there has been study of the ellipticity of anisotropy spots of CMBR, and the orientation of such ellipticity has also been discussed [10]. This study was motivated by the effects of geodesic mixing, though it has similarities with our technique in the sense of attempting to detect elliptic shapes and orientations of such shapes. However, a systematic study of general shape deformations and orientation resulting from an anisotropic expansion the universe during entire history of the evolution of density

fluctuations in the universe has not been carried out.

The possibility of anisotropic expansion of the universe has been discussed in the literature in different contexts. There are models which describe anisotropic cosmologies [11] and these have been investigated from the point of view of constraining the anisotropy parameters of the models from CMBR data [12]. The possibility of anisotropic expansion due to strings, walls and magnetic fields has also been discussed [13]. It has also been discussed that with some coupling between gauge fields and the inflaton, the anisotropy may persist through the inflation (avoiding the no-hair theorem [1]) and resulting power spectrum of fluctuations has been calculated [14]. We will not be discussing any specific model here for anisotropic expansion of the universe. We just assume that for whatever reason, if ever there was an anisotropic expansion of the universe in the history of the universe, from the beginning of the origin of density fluctuations (relevant to the observational scales at present) all the way up to the stage of last scattering, then we ask how one can probe it using shape analysis of patches (excursion sets) of CMBR fluctuations.

III. GENERATING EXCURSION SETS FOR SHAPE ANALYSIS

The main idea underlying our analysis is the following. If the density perturbations generated initially (say during inflation) are statistically isotropic, then they will continue to have an average spherical shape (statistically) if the expansion of the universe was always isotropic. But if the universe ever went through an anisotropic expansion, then these perturbations would get deformed in a specific direction [13]. For example, if the universe ever expanded differently in one direction from the other two then the *average* shape of these perturbations will become ellipsoidal, with the axes of the (statistical) ellipsoids all aligned. This average deformation will survive the later isotropic expansion at least till the time the size of the perturbation remains superhorizon. (Assuming that these small superhorizon fluctuations evolve linearly and undergo simple scaling with the expansion.) This means that any anisotropic expansion from the beginning of inflation to the surface of last scattering will leave their signature in the shapes of superhorizon perturbations in the CMBR. Fig.1 shows this basic physical picture where initially spherical fluctuations are shown to evolve with isotropic expansion of the universe and with a transient anisotropic expansion stage. The fluctuations remain spherical if the universe expansion was always isotropic. However, they deform to ellipsoidal shapes during an anisotropic expansion period (which, for simplicity, is taken here as faster expansion along the major axis of the ellipses shown). Subsequently the expansion of the universe becomes isotropic. However, the fluctuations retain their ellipsoidal shapes, with same geometry, as well as orientation. Note here we are referring to superhorizon fluctuations (of small amplitude), hence they are assumed to evolve linearly with the scale factor. This shape deformation information may also remain in the sub-horizon fluctuations due to linear evolution of the fluctuations. However, there may be causal effects, e.g. due to the presence of background fields, which may affect the shapes of these fluctuations. Though such causal effects will still remain uncorrelated over superhorizon scales. Hence they should not affect the statistical isotropy of the fluctuations. However, it seems simpler to rely on superhorizon fluctuations for the detection of anisotropic universe expansion. With high resolution data from Planck it will be important to consider shapes of sub-horizon fluctuations, especially as it will contain information about the dynamics of various causal factors present during the acoustic oscillations.

For an anisotropic inflation which later tends towards isotropy, deformation will be more for large size patches, those which exited the horizon during early stages of the inflation. The shape deformations will tend to zero for the small size patches, those which exit the horizon once the universe expansion becomes (almost) isotropic. Thus, a careful analysis of the shapes of patches of different sizes may be able to show this pattern in the CMBR sky of an anisotropic universe tending to an isotropic one (unless anisotropic expansion stage happened too early, followed by a very large duration of isotropic inflationary expansion). Any anisotropic expansion after the inflation (more precisely, after the generation of fluctuations) can always be detected by our method, as in this case patches of all superhorizon sizes will show similar deformation.

We look for these shape deformations in the over/under density patches with sizes greater than about 1° in the CMBR sky by measuring their extents along and transverse to a given axis. We consider a relatively thin strip along the equator of the CMBR sky (so that it is reasonably flat for projection on a plane), and analyze the extents of various patches along the latitudes (called as the X direction) and along longitudes (called as the Y direction). Thus our analysis is not very accurate for very large scale anisotropies for which one will need to analyze anisotropies in patches covering large parts of the sphere. If the universe ever expanded faster or slower along the polar axis compared to its expansion in the equatorial plane, then the shape deformations of density (temperature) fluctuation patches along this thin equatorial belt will be most sensitive to it. For example, the stretching of small patches at the equator will be simply proportional to the ratio of expansion factors along z axis that along the transverse equatorial plane. This is what we will assume in the following when setting constraints on the expansion factor anisotropy of the universe. Note that for patches of large angular scales this proportionality will not hold. We repeat this analysis for various orientations of the north pole in the CMBR sky, thereby probing anisotropic expansion in any possible

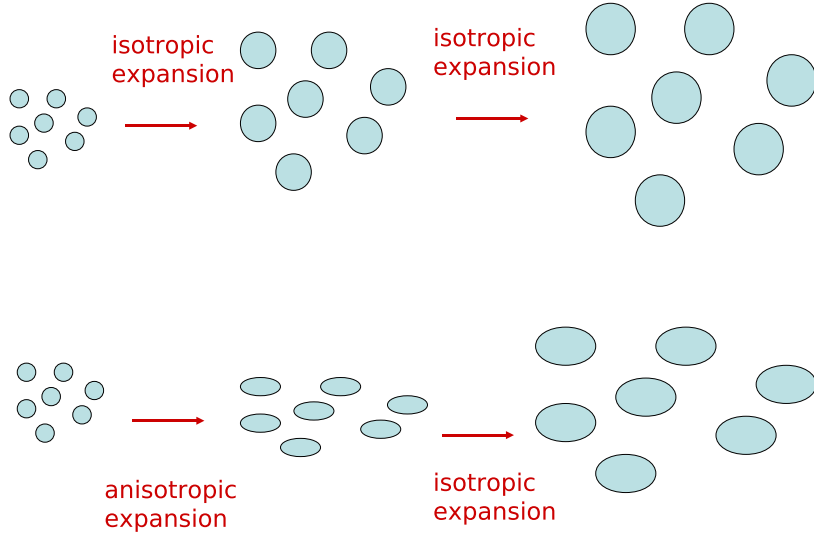


FIG. 1:

Basic physical picture of our model. Top part shows the evolution of initially spherical fluctuations during isotropic universe expansion. Fluctuations remain spherical. Bottom part shows the effects of a transient anisotropic expansion stage of the universe on the initially spherical fluctuations. Fluctuations become ellipsoidal with the same orientation, and these features are retained subsequently.

direction.

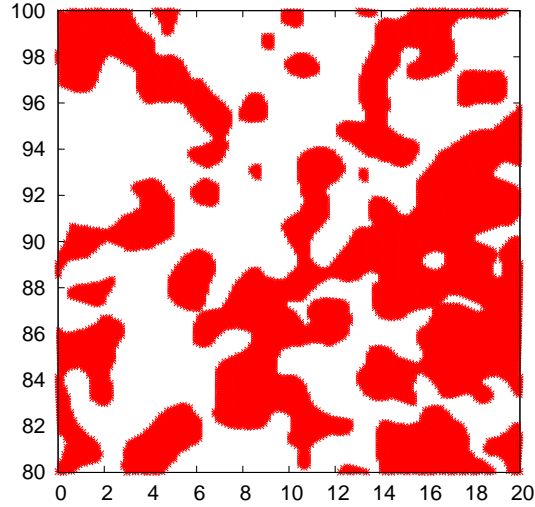


FIG. 2:

All the angles are in degrees. In all the figures, the X axis corresponds to $\phi \sin \theta$ and the Y axis shows θ . This figure shows the overdensity patches (excursion sets) in a $20^\circ \times 20^\circ$ region in the equatorial belt of CMBR sky (with a suitable threshold value).

We use WMAP 7-Year Data (ILC map) [15] for the analysis. However, we face a problem in applying our technique by using a thin strip along the equator. This is because the equatorial region with WMAP data is the most contaminated one with foreground noise. We avoid this problem by rotating the z axis (about the x axis) by 30° and by 70° , (due to special arrangements of pixels in HEALPix, some orientations are not convenient, e.g. 90°). Then we carry out our analysis by considering a strip along the (rotated) equator. There will still be some contamination from the intersection points with the original equator, but hopefully its contribution will be relatively small. We choose a strip of width $\pm 10^\circ$ along this rotated equator, and choose CMBR fluctuations above/below a particular value thereby forming the excursion sets. Fig.2 shows a small $20^\circ \times 20^\circ$ region in this equatorial belt. Filled patches seen in Fig.2 correspond to temperature anisotropies of magnitude $(0.02 - 1) \times (\Delta T)_{max}$ where $(\Delta T)_{max}$ is the maximum magnitude of CMBR temperature anisotropy in this patch. As one can see, the patches appear randomly shaped and sized. This picture is projected on a plane to calculate the X and Y extents of the filled patches (with the X extent being taken as $\phi \sin \theta$ and the Y extent is taken as θ). θ and ϕ are the polar and azimuthal angles respectively. Thus, though we denote X and Y in terms of $\phi \sin \theta$ and θ in degrees, these actually represent length scales with suitable multiplication of radius of a sphere representing last scattering surface.

We see that actual fluctuations in CMBR in Fig.2 do not look anywhere as simple as the geometrical fluctuations in Fig.1, and one cannot straightforwardly look for the shape deformations, and any overall orientation of such deformations. Even though fluctuation patches in Fig.2 appear of arbitrary shapes, statistically averaged shape of the fluctuations will be spherical (isotropic), and main idea of our approach is to detect any deformations in this *statistically averaged shape* of the fluctuation patches. Thus, isotropic expansion will stretch the fluctuations symmetrically, leading to the statistically averaged shape remaining spherical, while any anisotropic expansion stage stretches the fluctuations asymmetrically. The statistically averaged shape will become ellipsoidal if the expansion is asymmetric along one direction.

IV. FOURIER TRANSFORM TECHNIQUE

Detection of shape anisotropies using Fourier transforms can be done in different ways depending on what criterion one adopts to characterize the anisotropy [16–18]. The techniques of refs. [17, 18] are somewhat similar and here we will follow the approach used in [18] for analyzing anisotropic deformations in metallography. In ref. [18], a digitized image of the material was used and 2D Fourier transform of this image was calculated and subsequently thresholded to levels 0 and 1. Anisotropy in the Fourier space was then determined by the ratio of the widths of the histograms in the two directions.

Fig.3a shows the 2D Fourier transform of the picture in Fig.2 where we have used a suitable threshold to convert the values of the Fourier transform to 0 and 1. Fig.3b shows the plots of the histograms in the two directions (k_x, k_y) corresponding to Fig.3a. Solid curve and the dashed curves are the best fits to the histograms, which are Gaussian curves. The two plots completely overlap. The ratio of the widths of the Gaussians in k_x and k_y directions is

$$\frac{\sigma_{k_x}}{\sigma_{k_y}} = 1.03 \pm .02 \quad (1)$$

showing the statistical isotropy of the excursion sets in Fig.2. We mention here that the shapes of these two curves depends on the threshold values used for converting the Fourier Transform to levels 0 and 1. In our analysis (for all the figures) we have tried to fit (un-normalized) Gaussians as their widths and the normalizations provide a quantitative characterization of the anisotropy. However for certain cases (e.g. in Figs.10, and 11 below) it is not possible to fit Gaussians. More appropriate curves are of the shape of Woods Saxon potential and that is what we use. In such cases, we use suitable threshold values which maximize the difference between the two histograms, while the histograms remain reasonably smooth curves.

V. SHAPE ANALYSIS IN THE PHYSICAL SPACE

We now describe our technique for detecting shape deformations directly in the physical space. Clearly, what one wants to know is the average width of the fluctuations in X direction and compare it with the average width in the Y direction. That will work well if fluctuations were of specific geometrical shapes and sizes and not for fluctuations as in Fig.2. What one wants to know here is the distribution of widths in the X direction and compare it with the distribution of widths in the Y direction. For this we proceed as follows. We divide the entire 20° wide equatorial belt (with θ within $\pm 10^\circ$ about the equator, and ϕ ranging from 0 to 360°) into thin slices (varying from 0.02° - 0.1°) in X and Y directions (to increase statistics). Using these slices, we determine the X and Y extents of various

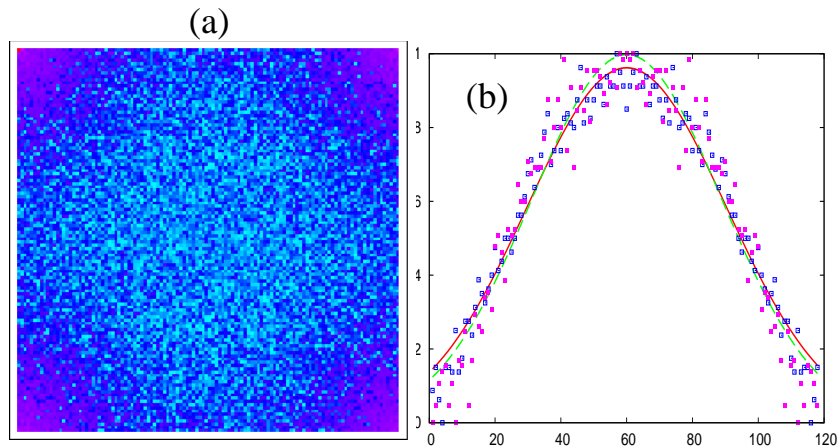


FIG. 3:

(a) shows the 2D Fourier transform of the picture in Fig.2 with an appropriate threshold to levels 0 and 1, with the horizontal and the vertical axes representing k_x and k_y (this picture is shown only to qualitatively see the isotropy of the scatter plot, hence we do not show axis markings here). (b) shows the histograms in the two directions for (a). Solid and dashed curves (which completely overlap) are best fits to these histograms.

filled patches. This procedure is shown in Fig.4a for the $20^\circ \times 20^\circ$ region of Fig.2. (Note that X with $\sin(\theta)$ factor, and Y widths, represent distances on the sphere. However, we keep referring to these in degrees.) We then plot the frequency distributions (histograms) of X and Y widths of the intersections of all the patches with these slices in this entire equatorial belt. For the isotropic case, we expect the X and Y histograms to almost overlap. Any relative shift, or difference, between the X and the Y histogram will imply the presence of an anisotropy, such as an anisotropic expansion. We mention that this fine slicing of the equatorial strip is done to simplify the shape analysis. The main idea is to get statistical information about X and Y widths of these random patches. The information on the nature of expansion will be contained in the distributions of each X and Y slice of the equatorial strip and collection of data from all the slices will therefore provide us with a good statistics.

Fig.4a shows these slices in the X and Y directions for the picture in Fig.2. Fig. 4b shows the frequency distributions (histograms) of the widths of the intersections of the slices with the filled patches (excursion sets) in X and Y directions for the entire equatorial belt. The solid curve shows the histogram of X slices of filled patches and the dashed curve shows the histogram for the Y slices. The horizontal axis corresponds to the widths of the slices in degrees (for X slices, it represents width using $\phi \sin \theta$), with histogram bin having width of 1° . The vertical axis gives the frequency N of the occurrence of the respective widths in all the slicings (X or Y respectively) of excursion sets in the equatorial strip. The error bars denote the statistical uncertainty of \sqrt{N} for the frequency N in each bin. We can see that the two histograms, corresponding to X and Y extents of the patches, are almost overlapping. This confirms the statistical isotropy of the fluctuations in Fig.2 (calculated here for the entire equatorial belt). This is consistent with the isotropy seen in Fig.3 using the Fourier transform of the $20^\circ \times 20^\circ$ region of Fig.2. (We mention here that the peak at about 1° in Fig.4b presumably corresponds to the smoothing of WMAP data below this scale.)

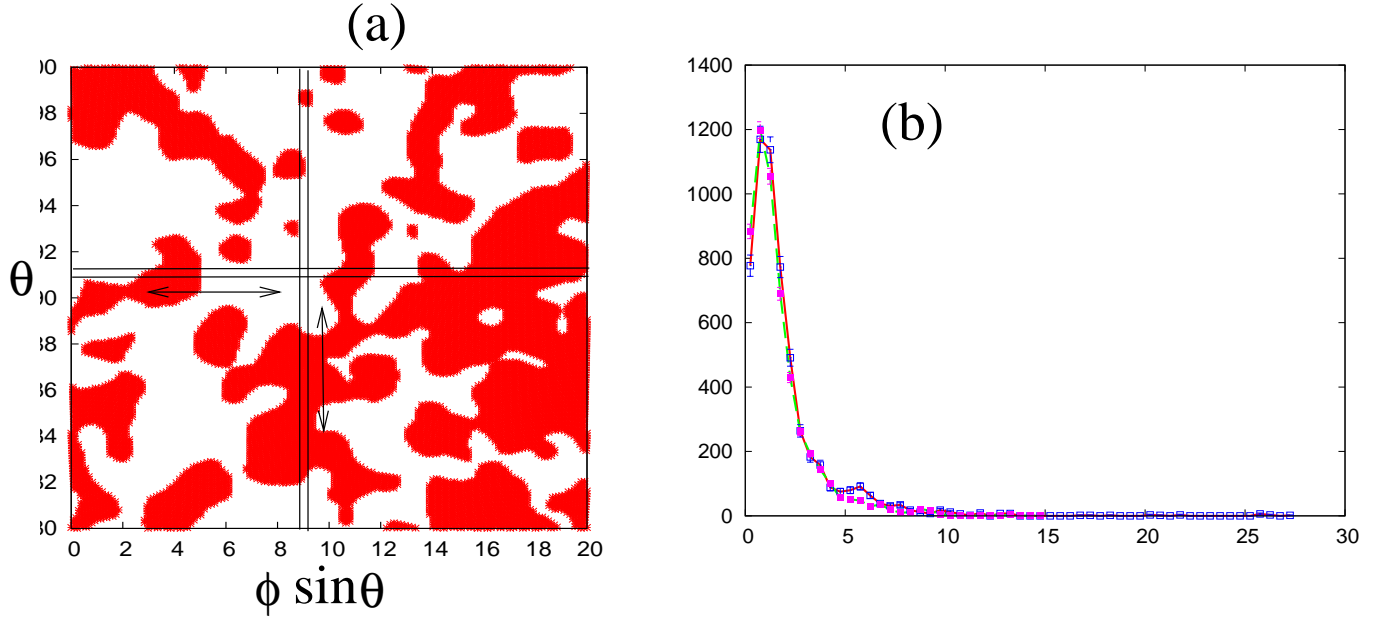


FIG. 4:

(a) Slicing used along X and Y axes for the $20^\circ \times 20^\circ$ region in Fig.2. Widths of filled patches (excursion sets) intersected by the slices are determined and histograms are calculated for the distribution of these widths in X and Y directions. (b) shows plots of these histograms of the widths of filled patches obtained using the entire equatorial belt with a width of 20° (along longitude). X axis represents widths of patches. Bin width is taken as 1° . Smooth curves join the points which are marked with corresponding (\sqrt{N}) error bars. Distribution for width along X ($\phi \sin \theta$) is shown by solid plot and distribution for width along Y (θ) is shown by the dashed line.

VI. CONSTRAINING ANISOTROPIC EXPANSION

To determine the level of isotropy which is implied by the overlap of the two histograms in Fig.3 and in Fig.4, we introduce artificial stretching in the CMBR patches in the following manner and repeat the above analysis for this *stretched* data. To *simulate* stretching by a factor α we simply multiply the Y coordinate (i.e. θ) for each point in the equatorial strip used above by a factor $\alpha \times \frac{|y|}{10^\circ}$. Here y denotes the value of θ in degrees measured with respect to the equator, with $-10^\circ \leq y \leq 10^\circ$ for the above equatorial strip. This stretching represents an anisotropic expansion of the universe along the polar axis compared to the expansion in the equatorial plane by a factor α . Note again that this simple scaling expression works approximately fine for a relatively thin strip along the equator. For strips having larger widths along the longitudes, the y coordinates of different patches will be scaled by a more complicated factor.

Fig. 5 shows this artificially stretched patch corresponding to the patch shown in Fig.2. The stretching factor is $\alpha = 2$ for Fig.5. For the consistency of the analysis we take the 20° wide entire equatorial strip from this stretched data set (the stretched strip now spans 40° width along the longitude for $\alpha = 2$). We first repeat the analysis of section IV by calculating the 2D Fourier transform of the picture in Fig.5, with suitable threshold for levels 0 and 1 and then calculating histograms of these values in the two directions. Similarly the analysis of section V is repeated for Fig.5 by slicing the entire (stretched) equatorial strip in X and Y (i.e. $\phi \sin \theta$ and θ) directions and determine corresponding histograms for widths of the filled patches. The results are shown in Fig.6. Fig.6a shows the Fourier transform of the picture in Fig.5 and Fig.6b shows the histograms calculated for this 2D Fourier transform as in Fig.3. We see that these histograms do not overlap showing the anisotropy arising from the stretching in Fig.5. The ratio of the widths of the Gaussians in k_x and k_y directions is $\frac{\sigma_x}{\sigma_y} = 1.04 \pm .04$. Anisotropy of Fig.5 is reflected here in the fact that the normalizations of the two Gaussians are different. Ratio of these two normalizations is $0.85 \pm .01$.

Similarly, Fig.6c shows the histograms resulting from the analysis of section V applied to the stretched equatorial

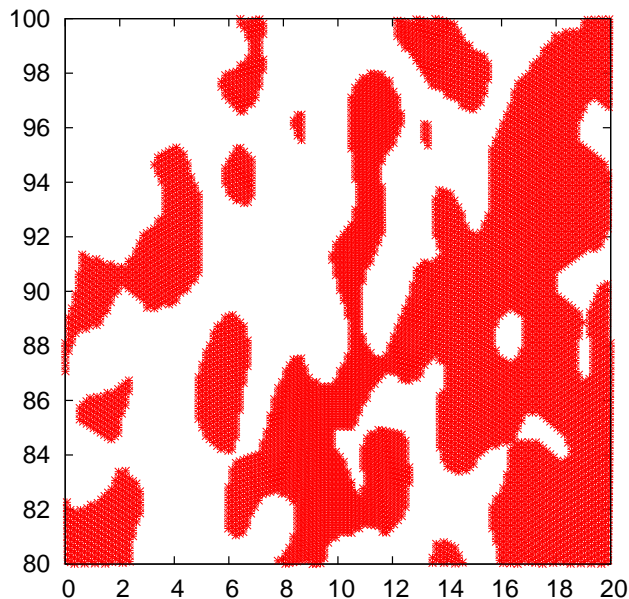


FIG. 5:

This figure shows the overdensity patches (excursion sets) in a $20^\circ \times 20^\circ$ region in the equatorial belt of CMBR sky after being stretched by factor 2 along the z axis.

belt. Again, the solid and dashed curves correspond to the X and Y histograms respectively. We see here also that the two histograms do not overlap and the difference is significant. The X (i.e. $\phi \sin \theta$) histogram fall above the Y (i.e. θ) histogram in the first few bins which is due to the fact that we have stretched all the patches thereby reducing the number of patches with small Y width. But for larger widths we have the Y histogram crossing and remaining above the X histogram which implies that we have more patches with larger width in Y slices. Note incidentally that the peak in the dashed curve (θ histogram) has shifted to larger widths by about a factor of 2 which is the factor of stretching of patches for Fig.5.

We mention here that we are not trying to deduce a number similar to the widths (or normalizations) of the histograms in Fig.3b, for some suitable widths of the curves in Fig.6c which can be compared for the X and Y distributions leading to a simple quantitative characterization of the anisotropy. This is because the precise nature of difference expected between the two histograms in Fig.6c is not easy to relate to the stretching factor α as it may also depend on the geometrical shapes of different random patches. For example, in the plots in Fig.6c, there are significant changes in the two distributions at larger angular scales, say, $10^\circ - 20^\circ$. However, these are dominated by fluctuations. Also, as mentioned above, at this stage our technique is not accurate for large scales. As we will see in later sections where simulated fluctuations of various geometrical shapes are analyzed, the changes in the X and Y histograms for pictures similar to Fig.5 are of very different nature. Unless one understands how the entire curve depends on the geometry, orientation, and distribution of the patches, it does not seem useful to devise any parametrization of these curves. For us, the significant point is that a stretching factor of $\alpha = 2$ produces X and Y histograms which are clearly distinct, beyond the error bars. A comparison with Fig.4b for the actual CMBR data implies that in the entire history of the universe, any anisotropy in its expansion along the z axis is bounded by $\alpha < 2$. In this sense of comparing the two distributions, our technique remains semi-qualitative.

Even with this limitation, it is important to appreciate that this simple technique of shape analysis is able to answer an important question in an almost model independent manner. That is whether the universe ever expanded anisotropically almost from the beginning of inflation near $t \simeq 10^{-35}$ sec. all the way up to the stage of last scattering when the universe was 300,000 years old. We can try to put stronger constraint on the anisotropic expansion factor α . For this, we have repeated the analysis of Fig.6c with different values of α (including values of $\alpha < 1$). Figs.7a-d show the cases of α varying from 1.5 to 1.2. We see that the two histograms corresponding to X and Y widths of patches are clearly separated for $\alpha = 1.5$ and 1.35. However, for $\alpha \leq 1.3$ the differences in the two histograms is insignificant. It is important to note here that the most important, qualitative, signature of anisotropic expansion in our technique is the relative lateral shift of the curves of the X and Y frequency distributions. This is clearly seen in Fig.6c representing larger length scales in one direction compared to the other direction. This automatically is

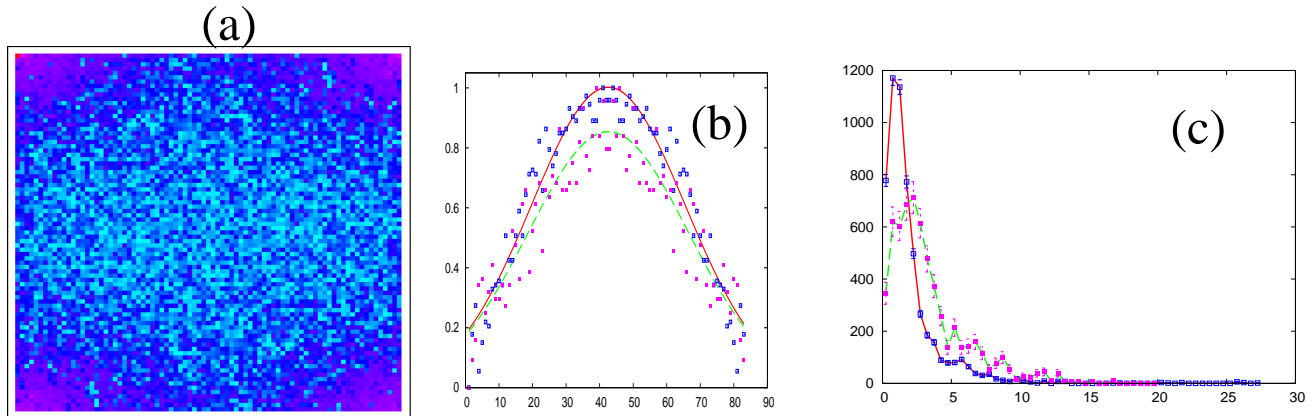


FIG. 6:

For the stretched CMBR data of Fig.5, (a) shows the 2D Fourier transforms, (b) shows corresponding histograms, and (c) shows plots of frequency distributions for widths of patches (excursion sets) of Fig.5 in X and Y directions for the entire equatorial belt.

correlated with change in relative heights of the peaks. Thus in Fig.7b though peak height are very different, our focus on detecting anisotropic expansion (here with $\alpha = 1.35$) is in the shift of the overall curve towards right. When we use smaller values of α , this lateral shift is not significant. With this, it seems reasonable to conclude that with our analysis technique, and with the present CMBR data, one can put a conservative upper bound of $\alpha < 1.35$ on the anisotropic expansion in the entire history of the universe (which could leave any imprints on the superhorizon fluctuations in CMBR, as explained above).

To rule out any chance coincidence, where any anisotropic expansion may have taken place along 45° from the z axis (which would stretch many patches by same factor in X and Y directions), we have repeated the above analysis of the patches along the equatorial belt for various orientations of the z axis. We have considered the original z axis of the WMAP data, and have also rotated the z axis (about the x axis) by 30° and by 70° (all the figures have been presented for this last case of 70° rotation, as mentioned above). The results are almost the same for all these cases as shown in Fig.4b, hence we do not show these plots. We have also repeated the analysis by using under-density patches in CMBR sky and the results are the same.

VII. ANALYSIS WITH SIMULATED FLUCTUATIONS

To check the importance of the geometry of these random patches in our technique, we have carried out the entire analysis of sections IV and V using simulated fluctuation patches with well defined spherical shapes. This has the advantage that one can distinguish between various scenarios of anisotropies, and see whether these different scenarios can be separately identified in our analysis. For this, we create a 3 dimensional cubic lattice in which overdensities of constant magnitude and specific geometric shapes are created at different locations. This represents a part of the universe enclosing the surface of last scattering. We then determine the shapes of the overdensity patches by embedding a surface of two-sphere S^2 (representing the CMBR sky) in this cubic region and recording the patches which are intersected by this S^2 . Fluctuation patches on this S^2 give us the simulated CMBR sky. Using this we repeat the above analysis of sections IV and V and determine histograms of 2D Fourier transforms and the histograms of widths of filled patches respectively. For the sake of simplicity of implementation, we do this analysis for $20^\circ \times 20^\circ$ patch near the equator for both the methods. By changing shapes of the fluctuations from spherical to ellipsoidal with constant, or varying ellipticity, and/or by making their distribution anisotropic, different initial conditions can be analyzed. We will discuss four broad cases in the following.

A. Spherical fluctuations, isotropic distribution

First we consider the situation when the fluctuations were generated by an isotropic process, and the entire evolution of the universe remains isotropic. In this case initial shapes of the fluctuations, as well as their distribution will be (statistically) isotropic, and this feature will be retained throughout the evolution of the universe leading to final

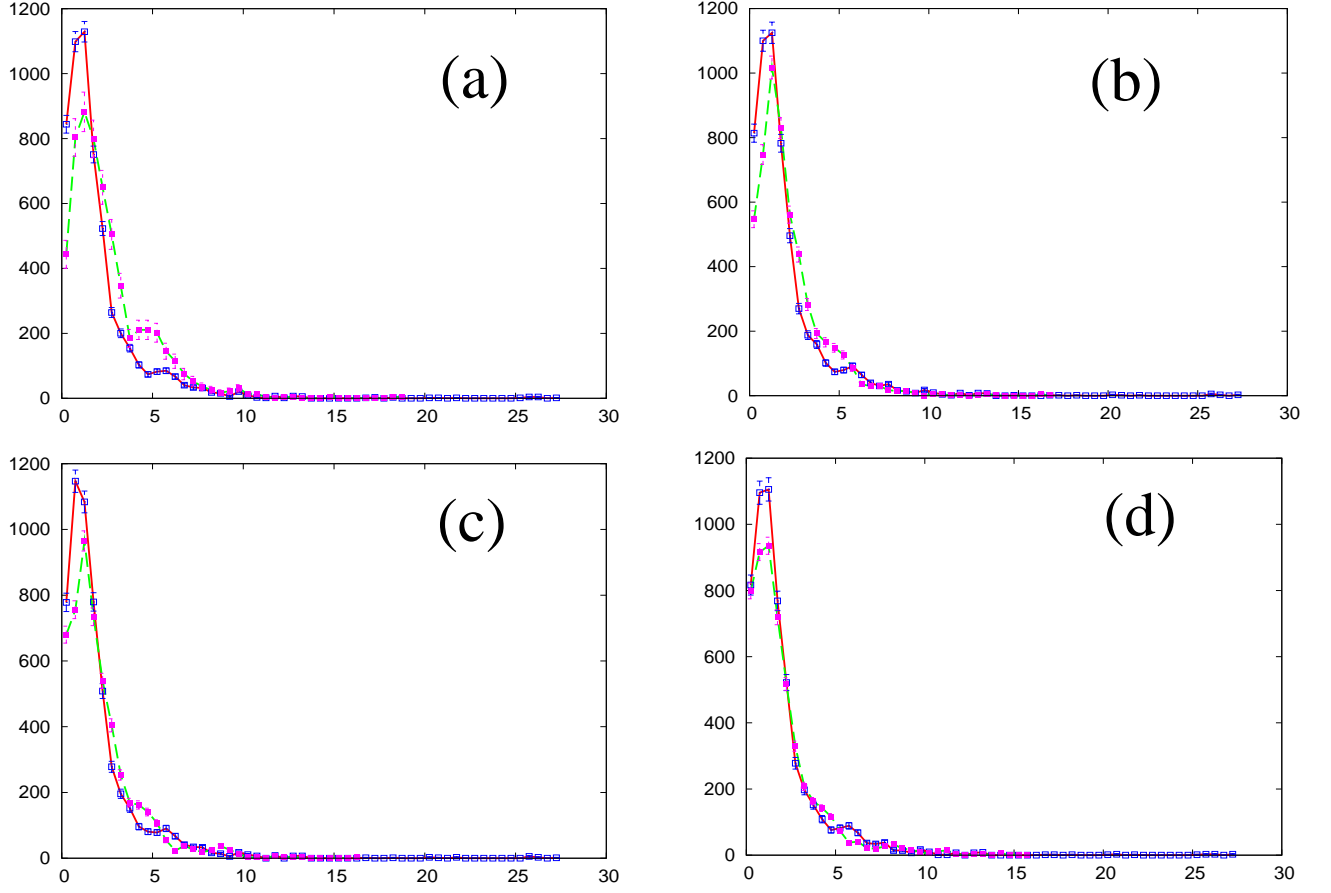


FIG. 7:

Plots of frequency distributions for CMBR data (as in Fig.6c) with stretch factor α ranging from 1.5 (a), 1.35 (b), 1.3 (c), 1.2 (d). X and Y width distributions are shown by solid and dashed curves.

spherical fluctuations. Also, the distribution of these fluctuations will remain isotropic. This situation is shown in Fig.8a. We have generated spherical fluctuations of different sizes. Note that geometrical spherical shape of these fluctuations is only supposed to represent statistically averaged shape of (the excursion set of) a realistic fluctuation. Also, note that all shapes may not appear spherical. This is because we are analyzing fluctuations on the surface of last scattering which represents intersection of a 2-sphere with spherical fluctuations present in the universe. Fig. 8b shows the 2D Fourier transform of (a) and (c) shows the corresponding histograms. Fig.8d shows the histograms of widths of intersections of the excursion sets in (a) with thin X and Y slices as discussed in section V. The respective histograms in the two directions overlap well showing the isotropy in (a). Note that there are larger errors in Fig.8d (and similarly for other figures for the simulated geometrical fluctuations) compared to, say, Fig.4b. This is because we are only using a $20^\circ \times 20^\circ$ region here with small number of fluctuation patches, compared to the full equatorial belt for Fig.4b. Ratio of the widths of the two Gaussian histograms in (c) (for 2D Fourier transform) is about $1.02 \pm .01$, again showing isotropy. It is clear from results shown in Figs.3,4 for real CMBR data that if we considered deformed (ellipsoidal) fluctuation patches with their orientations chosen randomly then again we will get overlapping histograms. Note that anisotropic expansion of the universe produces deformed shapes, all aligned in specific direction.

B. Spherical fluctuations, anisotropic distribution

It may be possible that the shape of the fluctuations is statistically spherical however their distribution is not isotropic. Though it is not clear what detailed model of the universe can give rise to such a situation, it may be possible, for example, if fluctuations were generated by topological defects whose production was not isotropic due to some biasing field. Seeding of topological defects and density fluctuations arising from them are different physical

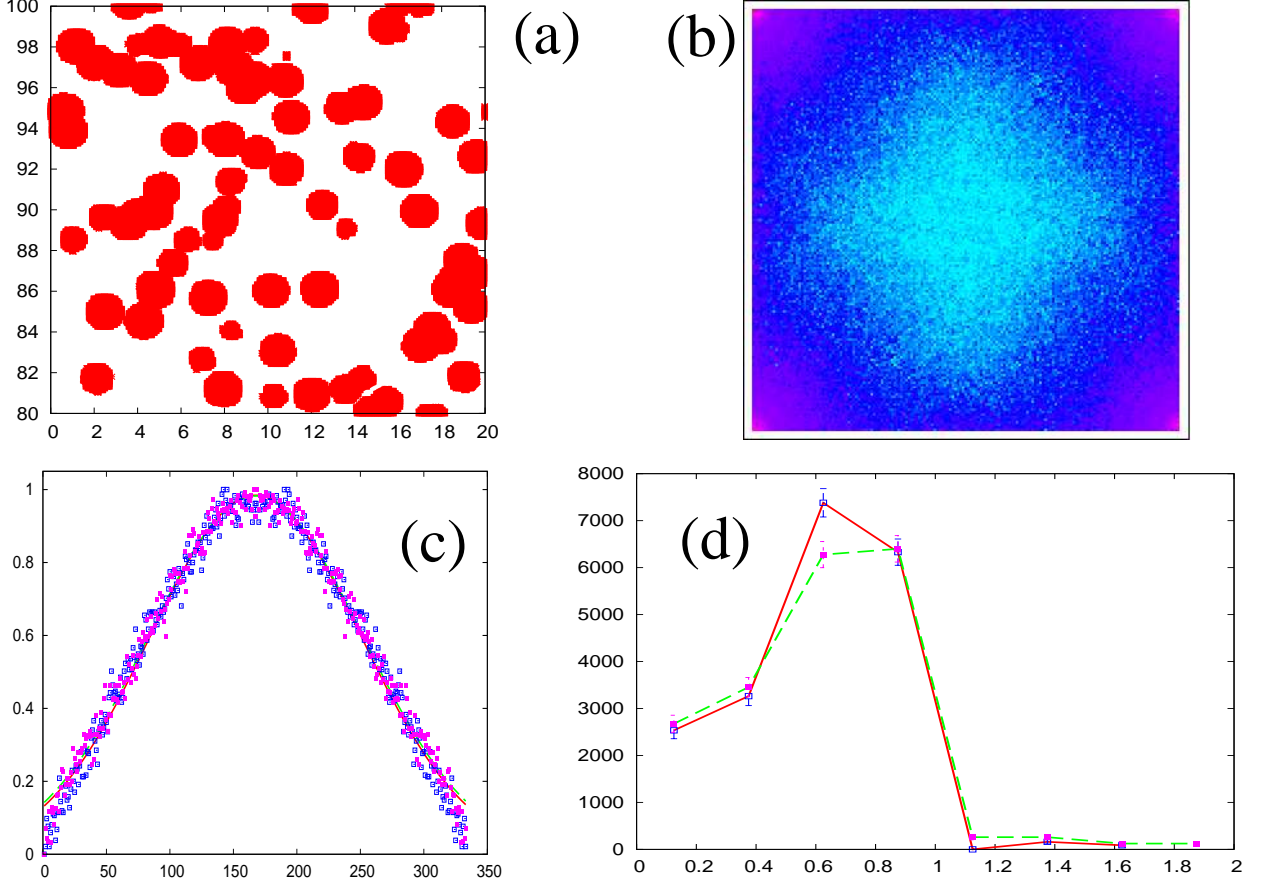


FIG. 8:

This figure shows various plots for the simulated geometrical patches. Again, all the angles are in degrees. (a) shows spherical overdensity patches distributed isotropically, (b) shows 2D Fourier transform (c) shows corresponding histograms, and (d) shows the histograms of the widths of the intersections of the fluctuation patches with the X and Y spatial slices in (a).

processes and may correspond to the present situation. Again we emphasize that our purpose is not to analyze specific models of density fluctuation production and their evolutions. We want to analyze different possibilities of anisotropies arising in the universe. Thus it is immaterial to us that defect mediated fluctuations are not consistent with CMBR measurements. Important point to recognize here is that this situation can only arise when the universe expansion remains isotropic at all stages. Because any anisotropy in the expansion will always lead to shape deformations in general. The anisotropic distribution (of spherical fluctuations), if at all possible, must result from the production mechanism of fluctuations.

Fig.9a shows spherical fluctuations which are distributed anisotropically. Fig.9b and 9c show the 2D Fourier transform and corresponding histograms. (d) shows the histograms of X and Y widths of the excursion sets in (a). In Fig.9c, the ratio of the widths of the Gaussians (for k_x and k_y directions in Fig.9b) is

$$\frac{\sigma_{k_x}}{\sigma_{k_y}} = 1.09 \pm .01 \quad (2)$$

We note that the 2D histogram method is sensitive to anisotropic distribution of the patches whereas the spatial width histograms are insensitive to it. This is as expected because spatial width method only analyzes the excursion sets and regions between these sets is not relevant. This is an important difference between the two techniques as our main purpose is to detect anisotropic expansion, and as explained above, the present case must correspond to the isotropic expansion of the universe.

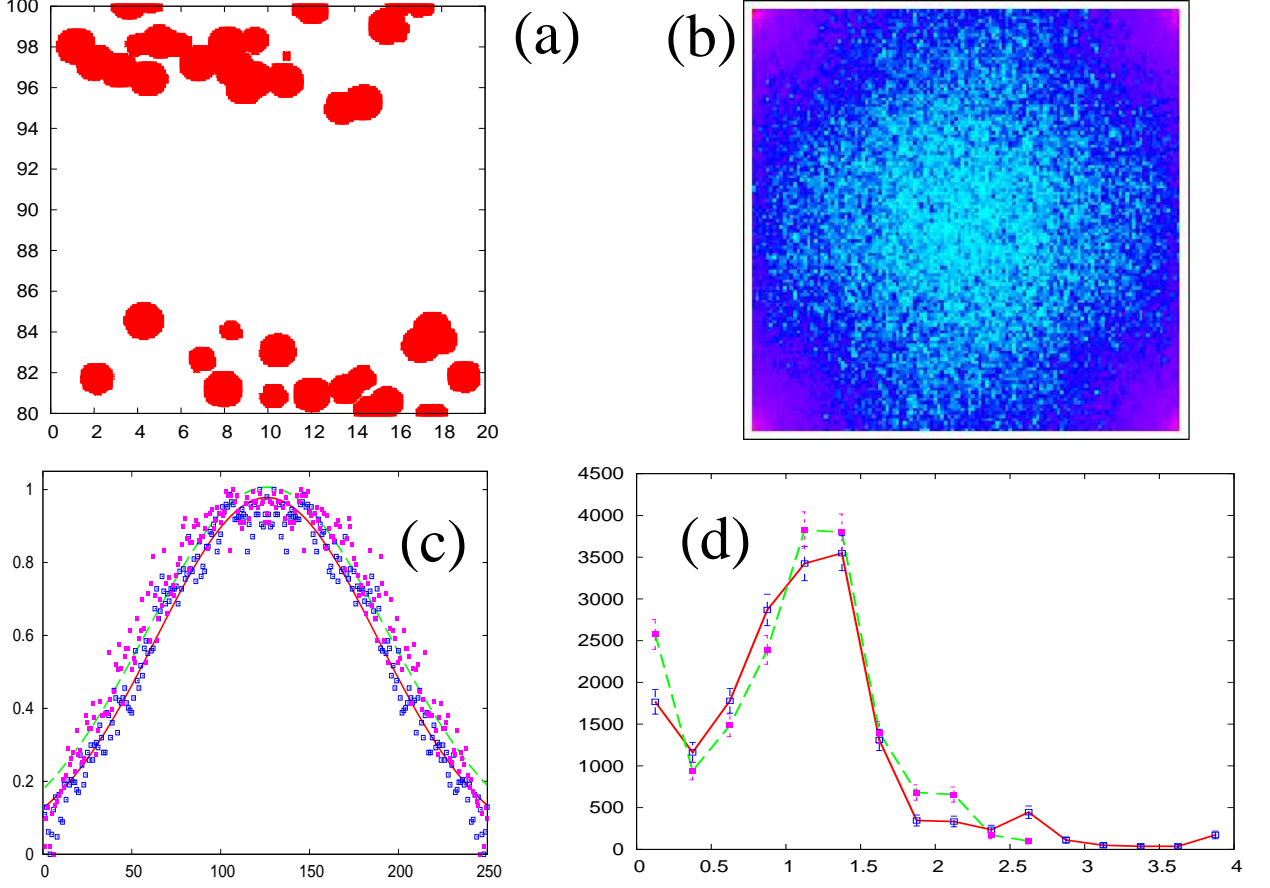


FIG. 9:

(a) shows spherical overdensity patches distributed anisotropically. (b) shows 2D Fourier transforms, (c) shows corresponding histograms, and (d) shows the histograms of the widths of the intersections of the fluctuation patches with the X and Y spatial slices.

C. Ellipsoidal fluctuations, fixed ellipticity

This should be the most standard situation when fluctuations are produced isotropically but they get stretched (and become ellipsoidal) during some early transient stage of anisotropic expansion of the universe. Thus, this is like the case depicted in Figs.5,6, (assuming inflationary fluctuations at generation were isotropic, but got stretched later). For this, we introduce the stretching in the simulated data set by a factor 2 (as for Fig.5). Fig.10a shows these ellipsoidal fluctuations which are distributed anisotropically (with anisotropic stretching the distribution automatically becomes anisotropic as in Fig.5). An important aspect of these shape deformation is that all these ellipses will have fixed ratio of the major axis to minor axis, this ratio directly referring to the relative expansion factors of the universe in the two directions. Fig.10b and 10c show the 2D Fourier transform and corresponding histograms, and Fig.10d shows the spatial widths histograms for the excursion sets of (a). Both, Figs.10c,d show distinctly non-overlapping histograms due to the anisotropy. The Histograms of 2D Fourier transforms are not fitted by Gaussians here. To fit these we use a Woods-Saxon potential shaped curve parametrized as follows.

$$f(x) = \frac{a}{1 + \exp(\text{abs}(x - x_0) - R)/\delta)} \quad (3)$$

here δ gives the width of the region where the function $f(x)$ decays (usually called the skin depth), and $2R$ characterizes the central flat part. x_0 gives the center. Ratios of R and δ for the two histograms in Fig. 10c are given below.

$$\frac{R_{k_x}}{R_{k_y}} = 1.011 \pm .003, \quad \frac{\delta_{k_x}}{\delta_{k_y}} = 1.94 \pm .04 \quad (4)$$

This figure shows that our technique works well for widely different geometries of patches, from completely random shapes in Fig.5 to well defined geometries in Fig.10.

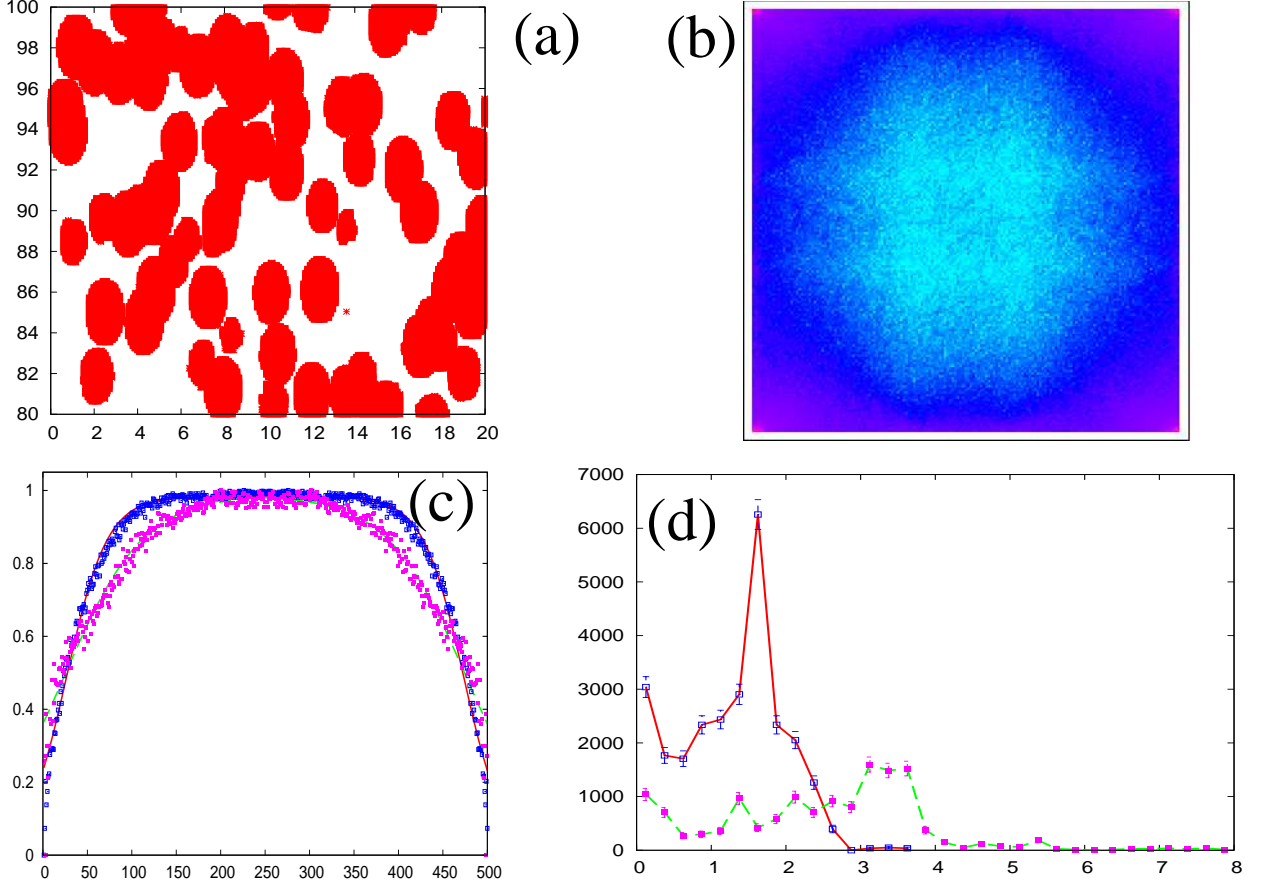


FIG. 10:

(a) shows ellipsoidal overdensity patches distributed anisotropically representing anisotropic expansion. (b) shows 2D Fourier transforms, (c) shows corresponding histograms, and (d) shows the histograms of the spatial widths of the fluctuation patches in (a).

D. Ellipsoidal fluctuations, varying ellipticity

We now consider the case when the fluctuations were anisotropic to begin with, possibly due to some biasing field, but the universe expansion remained isotropic throughout. Final fluctuation shapes will clearly be statistically anisotropic, relating to the initial anisotropy. It is important to see whether one can distinguish such a situation from the situation when fluctuations were initially isotropic but became deformed due to anisotropic expansion of the universe (as shown in Fig.10). We will argue in the following that it is indeed possible to distinguish these two cases with a little bit of physics input about the nature of processes generating density fluctuations.

Note that, as argued for Fig.10, when anisotropic shapes of fluctuations arise from anisotropic expansion, it leads to exactly same ratio of major to minor axis of the ellipsoids corresponding to the ratio of expansion factors of the universe in the two directions. This feature is extremely unlikely in any process of fluctuation production where anisotropy is arising due to some bias (e.g. some background field). Typically one will expect certain growth of the

anisotropy of the fluctuation in the background field implying that the anisotropy factor of the fluctuations should vary with the size of fluctuations. Note that there is range of sizes expected anyway as fluctuations are produced at different times and hence undergo different expansions. Such a class of different sized fluctuations will have same anisotropy factor. However, even for fluctuations produced at any particular given time, there is always a range of sizes of fluctuations for any physical mechanism, typically relating to some correlation length. These fluctuations of different initial sizes will undergo different evolutions in the biasing field (or due to biased production mechanism itself) and should end up with fluctuations of different sizes having different ellipticity factors. (If the anisotropic expansion factor changes in time then also one will get this type of situation which may be difficult to distinguish. However, in that case the pattern of ellipticity variation with size may be of a different nature.)

To model this situation we consider ellipsoidal fluctuations with different sizes having different ratios for the major to minor axis. Fig.11a shows distribution of such fluctuation patches. Fig.11b,c show the 2D Fourier transform and corresponding histograms and Fig.11d shows the histograms of spatial widths of the excursion sets. We note that though 2D Fourier transform method shows difference in the two histograms, thereby detecting anisotropy, the difference is qualitatively similar to that shown in Fig.10c. We again fit these two histograms using the Woods-Saxon function. Ratios of the relevant parameters (Eq.(3)) for the two histograms in Fig. 11c are given below.

$$\frac{R_{k_x}}{R_{k_y}} = 0.999 \pm .004, \quad \frac{\delta_{k_x}}{\delta_{k_y}} = 1.46 \pm .04 \quad (5)$$

Using this method, thus, it is hard to distinguish the case of Fig.10 from the present case. (Though, difference in Fig.10b and Fig.11b looks significant and may be of qualitative nature with a different characterization.) On the other hand, Fig.11d shows a qualitative difference between the X and Y histograms from that in Fig.10d in terms of shift of the peak for Y histogram from the one in X histogram. The shift of the peak by about factor of 2 in Fig.10 is directly related to the stretching of each patch by this factor. In contrast, in Fig.11 the peak reflects the fact that for small patches stretching is minimal. In that sense, for small scale patches, the structure of the two curves should be like in Fig.8. The stretching becomes significant only for large scale patches in Fig.11, consequently, the two curves differ for large scales. Though we do not know in detail how to characterize the shapes of the curves in terms of the geometry and sizes of patches, it is clear that there is a qualitative difference in the plots of Fig.11d and Fig.10d. This is very important as it shows the possibility that one may be able to distinguish between the anisotropic expansion case and anisotropic production process, both leading to finally anisotropic fluctuations.

VIII. CONCLUSIONS

We emphasize the most important part of our results, that a simple technique of shape analysis is able to answer an important question in an almost model independent manner. That is whether the universe ever expanded anisotropically almost from the beginning of inflation near $t \simeq 10^{-35}$ sec. all the way up to the stage of last scattering when the universe was 300,000 years old. Even with our qualitative approach of comparing the histograms in the two directions, we can conclude that our technique can rule out any anisotropic expansion of the universe in the past to less than 35%, (apart from any sufficiently early anisotropic stages of inflationary universe which are followed by very long, isotropic inflationary stage). In particular any anisotropic expansion stage after the end of inflation (or after the end of generation of fluctuations) is certainly restricted to $\alpha < 1.35$. With Planck data one should be able to do shape analysis of patches with high resolution. It will be specially important to do the shape analysis of sub-horizon fluctuations as that can provide additional information about the dynamical details of the evolution of subhorizon fluctuations such as any background fields, viscosity etc.

A major drawback of our present analysis is its restriction to relatively small angular scale (which is tentatively taken to be about 20° here). Thus, claims of anisotropy at quadrupole level in the literature are not examined by our analysis at present. Clearly this is physically very interesting case to check as any early anisotropic stage of the inflationary universe, which eventually turns into isotropic expansion, will lead to anisotropic shapes of patches at large angular scales (those which exited horizon early during inflation) while patches at small angular scales will be isotropic in shapes. We are working on improvement of our techniques for larger angular scales, and also trying to get better control on statistical fluctuations in our plots.

We mention here that this technique of identifying anisotropic early expansion by shape analysis of superhorizon fluctuation regions has a natural application to the physics of relativistic heavy-ion collision experiments (RHICE). Measurements of elliptic flow in non-central collisions in these experiments has provided a wealth of important information about initially anisotropic expansion of the anisotropic plasma region, such as equation of state, viscosity etc. Recently, we have argued that there are certain similarities in the physics of density fluctuations in the universe and in RHICE, in particular, relating to the presence of superhorizon fluctuations [19]. Thus, the technique presented

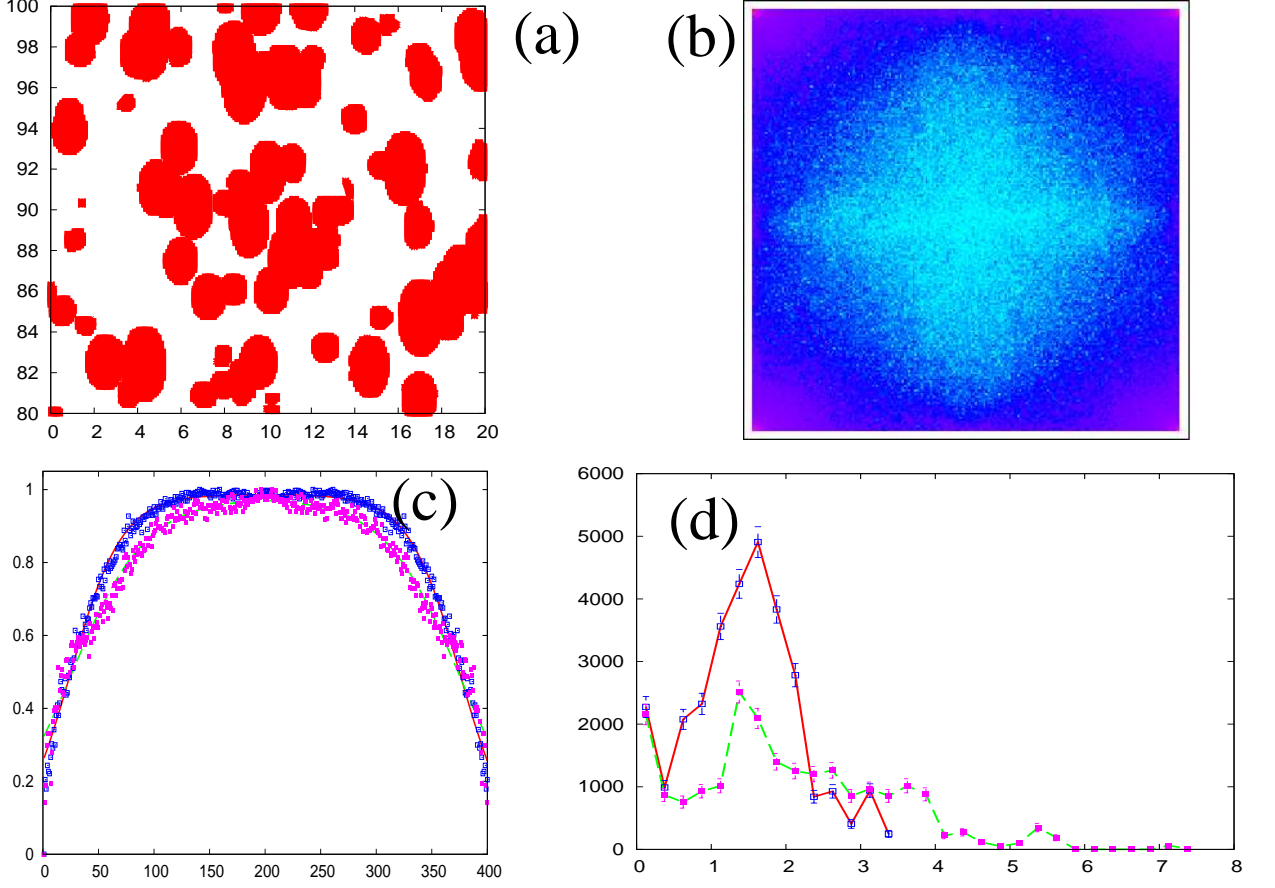


FIG. 11:

(a) shows ellipsoidal overdensity patches with varying anisotropy factors. (b) shows 2D Fourier transforms, (c) shows corresponding histogram, and (d) shows histogram of the spatial widths of the fluctuation patches in (a).

in this paper, when suitably applied to the shape analysis of large wavelength energy/number density fluctuation regions in RHICE, may yield important information about the early anisotropic expansion of the plasma. We will report this work in a future publication. This technique has obvious applications for other systems such as in condensed matter physics, for example in studies of growth of domains during phase transitions especially in the presence of biasing fields.

Acknowledgments

We are very thankful to Tuhin Ghosh and Pramod Samal for help in accessing the CMBR data. We are very grateful to Raghavan Rangarajan, Tarun Souradeep, Arjun Berrera, Pankaj Jain, Sanatan Digal, Abhishek Atreya, Anjishnu Sarkar, and Ananta Mishra for useful discussions and comments. For processing CMBR data we have used the HEALPix package. We acknowledge the use of the Legacy Archive for Microwave Background Data Analysis (LAMBDA).

-
- [1] R.M. Wald, Phys. Rev. **D28** 2118 (1983).
 - [2] P. Jain and J. P. Ralston, Mod. Phys. Lett. **A14** 417 (1999); C. J. Copi, D. Huterer, and G. D. Starkman, Phys. Rev. **D70** 043515 (2004); P. K. Samal, R. Saha, P. Jain, and J. P. Ralston, Mon. Not. Roy. Astron. Soc. **396** 511 (2009).
 - [3] K. Land and J. Magueijo, Phys. Rev. Lett. **95** 071301 (2005).

- [4] A. de Oliveira-Costa, M. Tegmark, M. Zaldarriaga, and A. Hamilton, Phys. Rev. **D69** 063516 (2004).
- [5] J. Schmalzing, M. Kerscher, and T. Buchert, In *Varenna 1995, Dark matter in the universe*, pp 281-291, (Proc. of Int. School of Physics Enrico Fermi, Course 82, *Dark Matter in the Universe*, Varenna, Italy, Jul 25 - Aug 4, 1995, astro-ph/9508154
- [6] M. Migliaccio et al. Nucl. Phys. **B194**(Proc. Suppl.) 278 (2009); J. Schmalzing and K.M. Gorski, astro-ph/9710185.
- [7] J.V. Sheth and V. Sahni. astro-ph/0502105; C. Hikage et al. (SDSS Collaboration), Publ. Astron. Soc. Jap. bf 55 911 (2003).
- [8] I.S. Knyazeva, N.G. Makarenko, and L.M. Karimova, Astronomy Rep. **54** 747 (2010).
- [9] G. Rossi, P. Chingangbam, and C. Park, arXiv:1003.0272; P. Chingangbam and C. Park, JCAP 0912 (2009) 019
- [10] V.G. Gurzadyan et al. , Mod. Phys. Lett. **A20** 813 (2005).
- [11] See, Chapt. XI, *General relativity - an Einstein centenary survey*, edited by, S.W. Hawking and W. Israel, Cambridge University Press, Cambridge (1979); G.F.R. Ellis and M.A.H. MacCallum, Coomun. Math. Phys. **12** 108 (1969).
- [12] T. Ghosh, A. Hajian, and T. Souradeep, Phys. Rev. **D75** 083007 (2007).
- [13] R. V. Buniy, A. Berera, and T. W. Kephart, Phys. Rev. **D73** 063529 (2006).
- [14] T.R. Dulaney and M.I. Gresham, Phys. Rev. **D81** 103532 (2010).
- [15] Jarosik, N., et.al., 2011, Astrophys. J. Suppl. **192** 14 (2011); D. Larson et al., Astrophys. J. Suppl. **192** 16 (2011).
- [16] D.D. Feo, S.D. Nicola, P. Ferraro, P. Maddalena, and G. Pierattini, Pure Appl. Opt. **7** 1301 (1998); B. Josso, D. R. Burton, and M.J. Lalor, Mech. Syst. and Signal Process. **19** 1152 (2005).
- [17] M. Tunak and A. Linka, Fibers and Textiles in Eastern Europe, **15**, 64 (2007).
- [18] R. Holota and S. Nemecek, Applied Electronics, 2002, p:88
- [19] A.P. Mishra, R. K. Mohapatra, P. S. Saumia, and A. M. Srivastava, Phys. Rev. **C 77**, 064902 (2008); Phys. Rev. **C 81**, 034903 (2010); R. K. Mohapatra, P. S. Saumia, and A. M. Srivastava, Mod. Phys. Lett. **A26** 2477 (2011).